Knowledge-Based Segmentation for Tracking Through Deep Turbulence

Patricio A. Vela, Marc Niethammer, Gallagher D. Pryor, Allen R. Tannenbaum, Robert Butts, and Donald Washburn

***Abstract*—A combined knowledge-based segmentation/active contour algorithm is used for target tracking through turbulence. The algorithm utilizes Bayesian modeling for segmentation of noisy imagery obtained through longrange, laser imaging of a distance target, and active contours for tip tracking. The algorithm demonstrates improved target tracking performance when compared to weighted centroiding. Open-loop and closed-loop comparisons of the algorithms using simulated imagery validate the hypothesis.**

***Index Terms*—Active contours, Bayesian statistics, geometric flows, tracking, turbulence.**

I. Introduction

THIS BRIEF considers the problem of tracking a high-speed projectile using a laser-based imaging system. Due to the distance between the laser source and the target, atmospheric effects become an important factor to consider [1]. The effectively random nature of turbulence introduces a significant source of noise to the tracking process due to apparent motion of the target in the recorded image sequence. The measurement noise is a detrimental source of jitter for the tilt mirrors controlling the laser beam [2]. A technique for suppressing this noise during the image processing stage is given in what follows.

Prior work on laser-guided target tracking has focused on understanding the source of jitter and reducing jitter through controller design for the optical system [2], [3]. Although effective plant and controller design lead to performance improvements, turbulence effects are a consistent source of noise not related to the physical process of tilt stabilization, which is what an effective tilt controller design typically corrects for. Related work on target tracking involves estimation and filtering algorithms for the tracking signal in order to guide a target to destroy another target [4], [5] with the sensor typically being radar. The focus of this brief is on the utilization of probabilistic image processing algorithms to provide spatio–temporal filtering of the image signal itself, and not of the resulting track signal. We will show that active contour methodologies may be naturally combined with this.

Many of the problems associated with noise and uncertainty found in imaging through turbulence are also common in biomedical imaging. The use of knowledge-based image processing techniques is commonly practiced [6]–[8] as is the use of active contours [9]. Consequently, the application of the aforementioned algorithms to target tracking should be fruitful. In [10], the authors apply statistical techniques with active contours to improve the segmentation of astronomical imagery, which also exhibits turbulence induced speckle and noise.

1) Modeling and Simulation Environment: The focus of this brief is on the image processing algorithms involved, therefore, detailed description of the physical modeling and image generation is omitted. Open-loop analysis was done using simulated imagery provided by the Optical Sciences Company (tOSC), which specializes in theoretical and experimental electro-optics. The simulated environment used for closed-loop analysis utilizes the *tempus* simulation environment and the *Wavetrain* adaptive optics model of the MZA Corporation.

Fig. 1 depicts the physical setup of the system. The laser-based imaging system is located on a moving platform whose goal is to autonomously track a distant target. The platform is equipped with a beam steering mirror to compensate higher order aberrations caused by atmospheric turbulence, a high-bandwidth steering mirror which is used to aim the laser for tracking purposes and an imaging sensor which picks up the return signal of the laser to generate an image of the target. In simulation, the target is equipped with a sensor, called the *target board*, which provides a reference signal for performance evaluation of the algorithms. The processes described in this brief focus on recovering a smooth and reliable track signal from the temporal image sequence.

2) Organization of This Brief: Section II briefly describes the knowledge-based segmentation algorithm. Section III briefly outlines the active contour method. The application of said algorithms to target tracking are discussed in Section IV, including comparison to a weighted centroiding technique. Both open-loop and closed-loop results are given, demonstrating the relative performance of the various tracking algorithms. A short conclusion and future work follows in Section V. In particular, we describe the possibility of putting dynamics directly into the active contour model as in [11] and [12].

II. Knowledge-Based Segmentation

A typical approach to target tracking involves smoothing the image to minimize the effect of noise, followed by thresholding to determine the target area. Turbulence induced image noise is nonadditive [1], therefore, smoothing techniques applied to the image directly do not reduce noise in a physically meaningful manner. Second, the dynamic nature of turbulence results in an image sequence whose peak intensities can have high variation from frame to frame, meaning that a constant threshold does not work well over a diverse set of turbulence scenarios. This section describes a statistical segmentation method which effectively operates as an adaptive threshold algorithm, thus providing a level of robustness to turbulence effects. Smoothing

Manuscript received August 18, 2005. Manuscript received in final form January 2, 2007. Recommended by Associate Editor S. Weibel. This work was supported in part by grants from MRI-HEL and AFOSR.

P. A. Vela, M. Niethammer, G. D. Pryor, and A. R. Tannenbaum are with the School of Electrical and Computer Engineering, Georgia Institute of Technology, Atlanta, GA 30332-0250 USA (e-mail: tannenba@ece.gatech.edu).

R. Butts and D. Washburn are with the Air Force Research Laboratory, Directed Energy Directorate, Kirtland Air Force Base, Albuquerque, NM 87117 USA.

Digital Object Identifier 10.1109/TCST.2007.899723

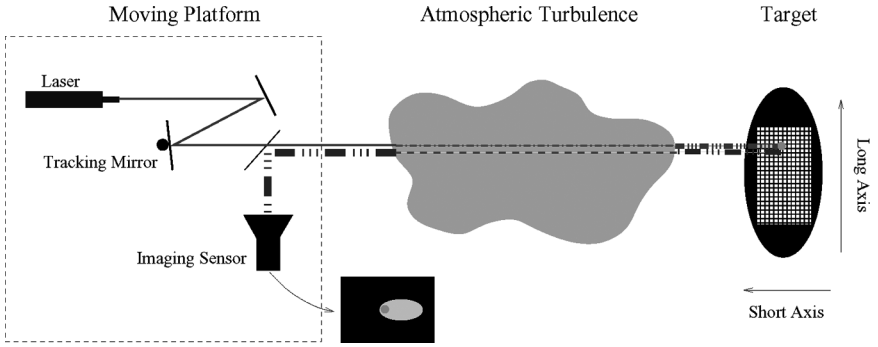

Fig. 1. Target tracking setup.

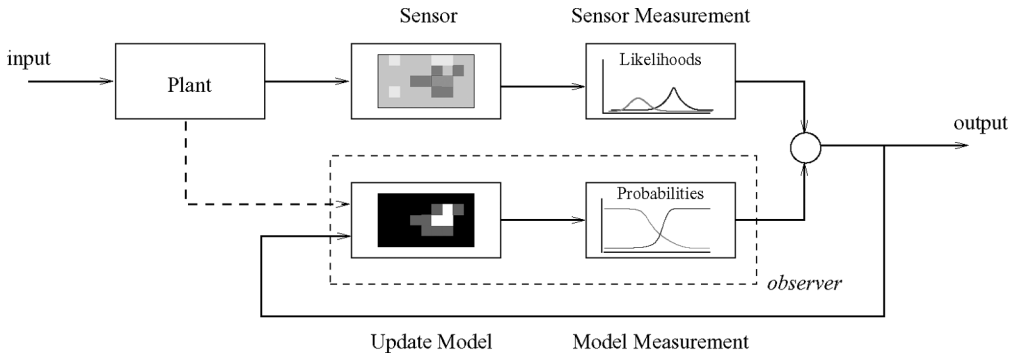

Fig. 2. Observer model for knowledge-based segmentation.

is performed on the probabilistic image model, which can be rigorously motivated using the Markov Random Field Theory [13], [14].

The knowledge-based segmentation algorithm used here relies on statistical analysis of the image sequence with segmentation done through a *maximum a posteriori* (MAP) approach. The MAP segmentation algorithm with Bayesian update, as implemented for image processing, is an adaptive thresholding algorithm that has found much success in processing noise corrupted imagery [15], [16]. The knowledge-based segmentation technique itself is an observer-based estimation algorithm using Bayesian modeling [13], where a probabilistic model is associated to the image sequence. Analysis is performed on the resulting probabilities, instead of on the original image. Fig. 2 depicts the observer-framework structure as a block diagram consisting of the plant, the sensor measurement, the update model, and the model measurement.

1) Model Description: The model description of the knowledge-based observer framework assumes that the image to process consists of M classes of gray levels $C = \{1, \ldots, M\}$, and that each class $c \in C$ is associated with a mean pixel intensity μ_c and standard deviation σ_c. Each class $c \in C$ has a probability field $\Pr(c_i = c)$ defined over the image domain, where i is a pixel location in the image domain and c_i is the classification of said pixel. The probability field gives the classification probability at each pixel location for each class. The goal of the segmentation process is to classify each pixel according to the most probable outcome.

2) Model Measurements: The model measurement for the problem described here is full-state measurement of the probability fields associated to the classes in C.

3) Sensor Measurements: The sensor measurements are not obtained directly from the imaging sensor, but are first passed through a preprocessing stage which converts the intensity values of the image into the probability space of the problem; this is known as the *sensor model* [13]. The probabilities are the likelihoods of classification based on the pixel intensities of the image. Each pixel intensity measurement v_i is treated as a random variable with a known distribution, independent of the other pixels in the image domain. The likelihood that a particular pixel intensity v_i is associated to a given class $c \in C$, $\Pr(v_i = v \,|\, c_i = c)$, follows a Gaussian distribution

$$\Pr(v_i = v | c_i = c) = \frac{1}{\sqrt{2\pi}\,\sigma_c} \exp\left(-\frac{1}{2}\frac{(v - \mu_c)^2}{\sigma_c^2}\right) \qquad (1)$$

with (μ_c, σ_c) the mean and standard deviation corresponding to the class $c \in C$. The sensor model assumes that the means and standard deviations for each class are constant over the imaging domain. Although not depicted in Fig. 2, the framework allows for adaptation of the statistical parameters underlying the sensor model, thus compensating for an incorrect model and/or time-varying image properties.

4) Correction Step: Given the classification probabilities of the current sensor measurement $\Pr(v_i = v | c_i = c)$, and also those obtained from the model measurement $\Pr(c_i = c)$, the

posterior probability of a pixel intensity being assigned to a particular class is given by Bayes' Rule

$$\Pr(c_i=c|v_i=v)=\frac{\Pr(v_i=v|c_i=c)\Pr(c_i=c)}{\sum_\gamma \Pr(v_i=v|c_i=\gamma)\Pr(c_i=\gamma)}. \quad (2)$$

Bayes' Rule plays the role of the correction step in the observer framework, as it attempts to resolve any discrepancies between the current sensor measurement and the current model measurement in the probability space.

5) Update Model: For open-loop analysis of an image sequence, the model update step is simply a static model where the posterior probabilities from the previous correction are used as the current probability model estimate. In closed-loop simulation, the actuation of the tilt mirrors for beam control causes the target image to shift around the image plane in direct proportion to the amount of mirror tilting. This effect must be considered in the update model, as denoted by the dashed line in Fig. 2, due to the spatial dependence of the probabilities defined on the image domain. The update consists of shifting the sensed probabilities according to the mirror tilts, effectively recentering the measurements. For the initial condition of the probability model, we use homogeneous probabilities.

Following [16], the posterior probabilities from (2) are calculated for each class, then smoothed and normalized to obtain $\widehat{\Pr}$. Smoothing of the posterior probabilities diffuses probability information to local neighboring pixels, thus giving the posterior probabilities spatial consistency in addition to the temporal consistency provided by Bayes' Rule. The smoothing step also suppresses any imaging noise being propagated through the observer framework. In order to account for a potentially incorrect sensor model of the likelihood Gaussian distribution, the means μ_c and standard deviations σ_c for the classes $c \in C$ are updated from their previous state according to the computed statistics of the current segmentation.

We should also note that implementing Bayes' Rule for a sequence of images without smoothing of the posteriors will tend to result in convergence to a fixed steady state, potentially incorrect. To prevent the segmentation process from converging to an incorrect steady state, smoothing of the posteriors is performed.

The final step of the process is to segment the object using the smoothed posterior probabilities, which are the outputs of the observer-based probabilistic model. The pixel i is assigned to the class with the maximal smoothed posterior probability

$$c_i^* = \arg\max_{c\in C} \widehat{\Pr}\,(c_i = c|v_i = v)\,. \quad (3)$$

Fig. 3 depicts a sample image and its segmentation via the MAP algorithm, where the classification set is $C = \{\text{target}, \text{background}\}$. The white area in Fig. 3(b) is classified as target, and the black area is classified as background. The MAP classification effectively segments the image by finding a suitably thresholded probability contour associated to the target class probability field (the target lies inside of this contour) or an active contour algorithm (see Fig. 3).

III. Active Contours

Active contours or *snakes* were introduced by Kass *et al.* [17] as energy minimizing splines in the 2-D image plane.

(a) (b)

Fig. 3. Example of MAP segmentation with target imagery. (a) Sample target image. (b) Segmentation of target image.

The energy to minimize is based on elasticity and rigidity constraints on the contour and the underlying image, defined such that the contour is attracted to desired image features. When applied to an image sequence, active contours employ image coherence in order to track features of interest over time. This ability of active contours to conform to various object shapes and motions makes them ideal for a variety of image processing needs, including segmentation, edge detection, shape modeling, and visual tracking. Moreover, they lend themselves to standard estimation and prediction techniques such as those based on Kalman filtering. Here, active contours are used to segment target from background in the image sequence.

The deformable contour model described in [18] and [19] is one of our key techniques for tracking. The method is based on Euclidean curve shortening evolution and on the theory of conformal metrics. The Euclidean curve shortening evolution defines the gradient direction whereby a given curve is shrinking most rapidly relative to Euclidean arc-length. The Euclidean arc-length is modified by a conformal factor adapted to the desired features of interest. Under the corresponding gradient evolution equations, the features to capture lie at the bottom of a potential well to which the initial contour will flow.

In [20] and [21], the authors introduce a snake model based on the level set formulation of the Euclidean curve shortening equation. More precisely, the model is

$$\frac{\partial \Psi}{\partial t} = \phi(x,y)||\nabla\Psi||\left(\text{div}\left(\frac{\nabla\Psi}{||\nabla\Psi||}\right)+\nu\right). \quad (4)$$

Here, the function $\phi(x,y)$ depends on the given image and is used as a "stopping term." For example, the term $\phi(x,y)$ may be chosen to be small near an edge, thereby impeding evolution when the contour gets close to an edge. One may take

$$\phi := \frac{1}{1+||\nabla G_\sigma * I||^2} \quad (5)$$

where I is the (greyscale) image and G_σ is a Gaussian (smoothing filter) filter [20], [21]. The function $\Psi(x,y,t)$ evolves in (4) according to the associated level set flow for planar curve evolution in the normal direction with speed a function of curvature, as introduced in [22] and [23].

It is important to note that the Euclidean curve shortening part of this evolution, namely

$$\frac{\partial \Psi}{\partial t} = ||\nabla\Psi||\text{div}\left(\frac{\nabla\Psi}{||\nabla\Psi||}\right) \quad (6)$$

is derived as a gradient flow for shrinking the perimeter as quickly as possible. A constant *inflation term* ν may be added to (4) in order to keep the evolution moving in the proper direction [20]. The sign of Ψ is negative in the interior and positive in the exterior of the zero level set.

To modify the model (4) in a manner consistent with curve shortening flow, consider the conformal length metric

$$ds_\phi = \left(x_p^2 + y_p^2\right)^{\frac{1}{2}} \phi dp$$

where $\phi(x, y)$ is a positive differentiable function and the curve in question is parametrized by p, e.g., $C = (x(p), y(p))^T$. The standard Euclidean metric is recovered with $\phi = 1$. To compute the corresponding gradient flow for shortening length relative to the metric ds_ϕ, define the modified length functional $L_\phi(t)$

$$L_\phi(t) := \int_0^1 ds_\phi = \int_0^1 \left|\frac{\partial C}{\partial p}\right| |\phi dp.$$

Taking the first variation of the modified length function and using integration by parts [19]

$$L'_\phi(t) = -\int_0^{L_\phi(t)} \left\langle \frac{\partial C}{\partial t}, \phi\kappa\vec{\mathcal{N}} - (\nabla\phi \cdot \vec{\mathcal{N}})\vec{\mathcal{N}} \right\rangle.$$

The direction in which the L_ϕ perimeter is shrinking as fast as possible is given by

$$\frac{\partial C}{\partial t} = (\phi\kappa - (\nabla\phi \cdot \vec{\mathcal{N}}))\vec{\mathcal{N}} \tag{7}$$

precisely the gradient flow corresponding to the minimization of the length functional L_ϕ.

The level set version of this is

$$\frac{\partial \Psi}{\partial t} = \phi||\nabla\Psi||\text{div}\left(\frac{\nabla\Psi}{||\nabla\Psi||}\right) + \nabla\phi \cdot \nabla\Psi. \tag{8}$$

The evolution of (8) should attract the contour very quickly to the feature lying at the bottom of the potential well determined by the conformal factor ϕ. As in [20] and [21], an inflation term ν may be added to obtain a modified model similar to (4)

$$\frac{\partial \Psi}{\partial t} = \phi||\nabla\Psi||\left(\text{div}\left(\frac{\nabla\Psi}{||\nabla\Psi||}\right) + \nu\right) + \nabla\phi \cdot \nabla\Psi. \tag{9}$$

Fast implementations of these snake algorithms based on level set methods are possible [22], [23]. The ability of the snakes to change topology and quickly capture desired features makes them an indispensable tool for visual tracking algorithms [24].

The active contour uses the posterior target probabilities as the grayscale image to use in (5). This provides a unique minima for the contour to attract to for segmentation of the target from the background. We should note that in this brief, we are in effect using global statistical information based on a Bayesian approach to drive our active contour models.

Finally, for tuning our gains in the Bayesian models we have used an active contour model "without edges" as in Chan–Vese [25] in order to separate the means and standard deviations for the Bayesian procedure. For example, to separate the means, we define the conformal factor as

$$\phi_a(u, w) = -\frac{1}{2}(u - w)^2. \tag{10}$$

Here $u = S_u/A_u$ and $w = S_w/A_w$

$$S_u = \int_{R^u} IdA \quad A_u = \int_{R^u} dA$$
$$S_w = \int_{R^w} IdA \quad A_w = \int_{R^w} dA$$

and R^u and R^w denote the domains inside and outside the curve, respectively. Computing the first variation and setting it to zero results in

$$\frac{\partial C}{\partial t} = -(u - w)\left(\frac{I - u}{A_u} + \frac{I - w}{A_w}\right)\vec{\mathcal{N}}. \tag{11}$$

IV. Target Tracking

Once the segmentation procedure defines a closed curve whose interior may be classified as the target, a track point must be determined. This section describes the technique used to compute the target signal using the knowledge-based segmentation algorithm, and will compare it to the target signal obtained from using a masked, weighted centroid algorithm. Two data sets are used for the comparison: one consists of pregenerated images for open-loop analysis of the tracking signal and the other is obtained through closed-loop simulation of engagement scenarios for the high-speed projectile through turbulence using the Wavetrain simulation of MZA Associates.

Target Determination: In practice, finding the front tip of the target provides the most reliable track point. The standard approach to computing this track point is to generate a mask by thresholding the image and using a weighted centroid of the masked image, biased towards the front of the missile. Closed-loop performance is typically good along the target's short axis, but can be poor for the long axis. The goal of introducing additional image processing is to improve the track signal along the long axis.

The knowledge-based segmentation/active contour algorithm generates a classification of target versus background, which can be used to mask the image, thus generating an image of the area classified as target only. A weighted centroid applied to the masked image finds a point on the target, from which the actual target tip may be sought. This may be accomplished by moving the track point along the long axis until the target probability drops to a predefined value or alternatively by using the geodesic (conformal) active contour segmentation methodology directly as previously described to find the target tip. Once the target tip is found, a track point is computed by averaging the tip with its neighboring tip points.

Fig. 4 demonstrates this process. The white contour surrounding the target is the previously found contour, and the black circle-plus is the initial target point obtained using the masked, weighted centroid, whereas the white circle-plus is the resulting track point after tip-seeking.

A. Open-Loop Analysis

For open-loop analysis, the algorithms may be analyzed using two measures, both involve comparing the resulting tracking signal to a scoring beam signal, which is provided by the simulation. The first method computes the correlation between the scoring signal and the appropriate tracking signal and the second calculates the standard deviation of the error

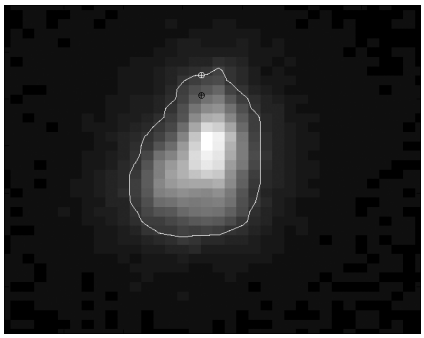

Fig. 4. Demonstration of tip-seeking for knowledge-based/active contour algorithm.

TABLE I
OPEN-LOOP TARGET TRACKING COMPARISON

Algorithm	Run	Axis	Cross Corr.	Std. Dev. (10^{-9})	% Improvement
CENT	01	long	0.831	634	–
		short	0.975	304	–
	02	long	0.838	635	–
		short	0.972	300	–
	03	long	0.827	652	–
		short	0.969	281	–
KBS/ACT	01	long	0.938	374	41.0
		short	0.980	292	4.0
	02	long	0.938	399	37.2
		short	0.980	276	8.0
	03	long	0.933	371	43.1
		short	0.975	264	6.1

TABLE II
CLOSED-LOOP TARGET TRACKING COMPARISON

Algorithm	Run	Axis	Std. Dev. (10^{-9}) 1000 frames	Std. Dev. (10^{-9}) 900 frames	% Improvement 900 frames
CENT	01	long	1015	982	-
		short	259	251	-
	02	long	1025	1017	-
		short	242	233	-
	03	long	1050	1028	-
		short	326	260	-
KBS/ACT	01	long	481	467	52.6
		short	259	248	0.0
	02	long	529	502	48.4
		short	249	249	-6.0
	03	long	558	508	47.0
		short	338	273	-3.7

between the tracking signal and the scoring beam signal once the two signals are in commensurate units.

Table I summarizes the performance results of the masked, weighted centroid (CENT) versus the combined knowledge-based segmentation/active contour algorithm (KBS/ACT) target tracking algorithm. In all cases, the first 15 track points out of 2500 total were discarded; a requirement due to the Bayesian learning process. When comparing the standard deviations, the KBS/ACT algorithm performed on average 6% better on the short axis and 40% better on the long axis. The correlations also show improvement, with higher correlations for both axes when compared to the centroid algorithm.

B. Closed-Loop Analysis

For closed-loop analysis the hit-point of the laser on the target board is used to measure performance. The standard deviation of the laser beam centroid on the target board is indicative of the degree of jitter in the closed-loop system. Table II summarizes the performance results of the two target tracking algorithms. There are two standard deviation measurements given, one which incorporates all 1000 frames of the simulation, the other which discards the first 100 frames from analysis. The early part of the signal tends to have high jitter due to the initial transient response of the closed-loop system. Comparing the standard deviations of the last 900 frames, the jitter for the KBS/ACT technique was slightly worse by about 3% for the short (easy) axis, but 49% better for the long (hard) axis. The slight discrepancies could be a result of using different simulations to generate the open-loop images versus the closed-loop images.

V. CONCLUSION

A combined knowledge-based and active contour segmentation algorithm for target tracking through turbulence was compared to a weighted centroid algorithm. This adaptive algorithm demonstrated significant improvements over the centroid algorithm. The long-axis performance results found in open-loop analysis of the target signal were reproduced in closed-loop simulation. Further simulated testing in more difficult scenarios is needed to verify the reproducibility of the results and the robustness of the algorithm prior to experimental verification.

In future work, we plan to employ the dynamic active contour models as in [11] and [12]. The hope is then we will no longer need the knowledge-based step at all.

ACKNOWLEDGMENT

The authors would like to thank T. Brennan and P. Roberts of tOSC and B. Fitzpatrick and Y. Wang of Tempest Technologies for their very helpful conversations and insights into high-speed projectile tracking.

REFERENCES

[1] M. Roggemann and B. Welsh, *Imaging Through Turbulence*. Boca Raton, FL: CRC Press, 1996.
[2] S. Steinvall, "Performance of laser tracking of small targets during turbulence and beam jitter," *J. Opt. Eng.*, vol. 43, no. 2, pp. 1609–1621, 2004.
[3] M. McEver, D. Cole, and R. Clark, "Adaptive feedback control of optical jitter using Q-parameterization," *J. Opt. Eng.*, vol. 43, no. 4, pp. 904–910, 2004.
[4] M. Ferdowsi, P. Maralani, and A. Sedigh, "Design of bearing-only vision-based tracking filters," *J. Opt. Eng.*, vol. 32, no. 2, pp. 472–481, 2004.
[5] B. Saulson and K. Chang, "Nonlinear estimation comparison for ballistic missile tracking," *J. Opt. Eng.*, vol. 43, no. 2, pp. 1424–1438, 2004.
[6] A. Achiron, S. Gicquel, S. Miron, and M. Faibel, "Brain MRI lesion load quantification in multiple sclerosis: A comparison between automated multispectral and semi-automated thresholding computer-assisted techniques," *Magn. Resonance Imag.*, vol. 20, no. 10, pp. 713–720, 2002.
[7] P. Teo, G. Sapiro, and B. Wandell, "Creating connected representation of cortical gray matter for functional MRI visualization," *IEEE Trans. Med. Imag.*, vol. 16, no. 6, pp. 852–863, Dec. 1997.
[8] J. Marroquin, R. Vemuri, S. Rotell, F. Calderon, and A. F. Bouzas, "An accurate and efficient Bayesian method for automatic segmentation of brain MRI," *IEEE Trans. Med. Imag.*, vol. 21, no. 8, pp. 934–945, Aug. 2002.
[9] M. Leventon, W. Grimson, and O. Faugeras, "Statistical shape influence in geodesic active contours," in *Proc. IEEE Conf. Vision Pattern Recog.*, 2000, pp. 316–323.
[10] E. Bourennane, C. Bondeau, and M. Paindavoine, "Region and Bayesian approaches for the restoration of images degraded byatmospheric turbulence," *Annales Telecomm.*, vol. 56, no. 9–10, pp. 538–549, 2001.

[11] M. Niethammer and A. Tannenbaum, "Dynamic level sets for visual tracking," in *Proc. Conf. Dec. Control*, 2004, pp. 4883–4888.
[12] M. Niethammer, A. Tannenbaum, and S. Angenent, "Dynamic geodesic snakes for visual tracking," in *Proc. IEEE Comput. Soc. Conf. Comput. Vision Patt. Recog.*, 2004, pp. 660–667.
[13] R. Szeliski, *Bayesian Modeling of Uncertainty in Low-Level Vision*. Norwell, MA: Kluwer, 1989.
[14] S. Li, *Markov Random Field Modeling in Image Analysis*. New York: Springer, 2001.
[15] S. Haker, G. Sapiro, and A. Tannenbaum, "Knowledge-based segmentation of SAR images," in *Proc. Int. Conf. Image Process.*, 1998, pp. 597–601.
[16] S. Haker, G. Sapiro, A. Tannenbaum, and D. Washburn, "Missile tracking using knowledge-based adaptive thresholding: Tracking of high speed projectiles," in *Proc. Int. Conf. Image Process.*, 2001, pp. 174–180.
[17] M. Kass, A. Witkin, and D. Terzopoulos, "Snakes: Active contour models," *Int. J. Comput. Vision*, vol. 1, no. 4, pp. 321–331, 1988.
[18] V. Caselles, R. Kimmel, and G. Sapiro, "Geodesic active contours," *Int. J. Comput. Vision*, vol. 13, pp. 5–22, 1997.
[19] S. Kichenassamy, A. Kumar, P. Olver, A. Tannenbaum, and A. Yezzi, "Conformal curvature flows: From phase transitions to active vision," *Archives Rat. Mech. Anal.*, vol. 134, pp. 275–301, 1996.
[20] V. Caselles, F. Catte, T. Coll, and F. Dibos, "A geometric model for active contours in image processing," *Numerische Math.*, vol. 66, pp. 1–31, 1993.
[21] R. Malladi, J. Sethian, and B. Vermuri, "Shape modelling with front propagation: A level set approach," *IEEE Trans. Patt. Anal. Mach. Intell.*, vol. 17, no. 2, pp. 158–175, Feb. 1995.
[22] S. J. Osher and J. A. Sethian, "Fronts propagation with curvature dependent speed: Algorithms based on Hamilton-Jacobi formulations," *J. Comput. Phys.*, vol. 79, pp. 12–49, 1988.
[23] J. A. Sethian, "Curvature and the evolution of fronts," *Commun. Math. Phys.*, vol. 101, pp. 487–499, 1985.
[24] A. Tannenbaum and A. Yezzi, "Visual tracking, active vision, and gradient flows," in *The Confluence of Vision and Control*, G. Hager and D. Kriegman, Eds. New York: Springer-Verlag, 1998, vol. 237.
[25] T. F. Chan and L. A. Vese, "Active contours without edges," *IEEE Trans. Image Process.*, vol. 10, no. 2, pp. 266–277, Feb. 2001.